KnE Materials Science

FibEnTech21
1st International FibEnTech Congress (FibEnTech21) New opportunities for fibrous materials in the ecological transition
Volume 2022

Knowledge E
enriching | engaging | empowering

Research article

Assessment of Autofocus Techniques for Isolated Cellulose Microfiber 3D Imaging by Digital Holography

Francisca Silva[1], Paulo Fiadeiro[2], and Elsa Fonseca[2]*

[1]University of Beira Interior, Covilhã, Portugal
[2]Fiber Materials and Environmental Technologies (FibEnTech-UBI) and University of Beira Interior, Covilhã, Portugal

Abstract.
Studying the three-dimensional structure of paper fibrous networks is an important step towards understanding the relationship between manufacturing conditions and the resulting microstructural and mechanical properties. Digital holography is a promising three-dimensional imaging technique enabling quantitative phase evaluation of micro and nano-fibres. One of the advantages of this high-resolution method is the ability to perform numerical refocusing at several depths from a single shot acquisition. In this work, the suitability of 22 focusing functions to accurately identify the positions of cellulose microfibers, using digital holography, was inspected. The best performing metrics were identified and the trade-off between metric accuracy and robustness to variable conditions and their computational complexity were discussed.

Keywords: digital holography, autofocus, cellulose microfibre, morphology, tomography

Corresponding Author: Elsa Fonseca; email: efonseca@ubi.pt

Published 10 August 2022

Publishing services provided by Knowledge E

Selection and Peer-review under the responsibility of the FibEnTech21 Conference Committee.

1. Introduction

Digital Holography (DH) is a powerful 3D imaging methodology that is particularly suited to microscopy applications [1]. This is achieved by encoding the wave field transmitted or scattered by an object in the form of an interference pattern with a reference beam. While in conventional imaging systems it is almost impossible to retrieve the correct focused image from a blur, with digital holography the image can be retrieved numerically at any distance from the hologram. DH also allows the reconstruction of various objects at different depths, beyond the depth of field limits of the system, through a technique called extended focus imaging [2]. Digital holographic microscopy (DHM) offers several significant advantages, such as the ability to acquire holograms quickly, availability of full amplitude, optical field phase information, and versatility of interferometric and image processing techniques [3]. Despite all the recognized advantages of this technique

over other more classic ones, there are also some disadvantages such as sensitivity to vibrations, depending on the optical setup used, existence of speckle noise due to the use of coherent light sources and the existence of reconstruction artifacts when using digital plane-wave holography in the in-line Gabor technique [4].

Getting three-dimensional and tomographic information on paper microstructures improves the understanding of the links between the manufacturing conditions and the consequent microstructural and mechanical properties of the paper fibrous networks [5]. In-line DH is characterized by its ability to image intensity and amplitude of objects with sub-micrometre resolution. Hologram reconstruction transforms also provide access to phase information and images of the spatial variations of phase changes of wavefronts in the optical field are easily created. Quantitative determination of phase changes is an integral part of in-line DHM so that, unlike the situation in conventional optical phase microscopy, a quantitative determination of the optical path through an object is easily performed. Classic interferometric phase shift measurements are capable of very high sensitivity but are often difficult to employ. The simplicity of this technique makes it of great interest to determine the extent to which accurate optical path measurements on micrometre-sized objects are possible [6]. Furthermore, the in-line configuration of DH enables highly compact setups, with digital autofocus capabilities. These features allow to overcome typical *runout* and *jitter* constraints inherent to conventional optical tomography [7]. These phenomena result from misalignments and vibrations in the signal acquisition phase due to sample rotation. The multi-view or phase reconstruction capability has the potential to allow the reduction of the number of acquisitions, making the recording process faster. It has recently proved to be possible to apply digital tomography techniques to microscopic plant fibres [7] and to single-mode optical fibres [8] with DH based on the Mach–Zehnder configuration. Also, the application of DHM to the (non-tomographic) study of cellulose nano-whisker aggregates revealed to be promising [9].

Aiming at developing a DH based microtomographic technique for isolated cellulose microfiber characterization, a set of optimization tasks are currently in process, were the selection of the most suitable autofocus technique is of critical importance. The pursued metric should be computationally simple while remaining effective and sufficiently precise for the correct localization of small objects immersed in a liquid or gel matrix medium. A special attention is devoted to sparsity metrics due to their small computational cost and potential to incorporate an advanced reconstruction procedure targeted at simultaneously reconstructing and focusing the complex object field by employing compressive sensing methods [10].

2. Material and methods

To test the selected focusing criteria, digital holograms of a set of objects including a USAF 1951 standard resolution target and two types of plant microfibers (eucalyptus and pine tree) were selected. An in-line Gabor DH setup with a He-Ne laser with $5\ mW$ and $632.8\ nm$ wavelength for sample illumination was used, as shown in Fig.1. The interference patterns were digitized by a Guppy Pro F-503 camera, having a CMOS sensor with a $2.2\ \mu m \times 2.2\ \mu m$ pixel size, using an acquisition mode with 2588×1940 pixels of resolution and 8-bit depth. Each hologram results from a pair of interference patterns, were the first is the test hologram, recorded with the sample in place, and the second is a reference hologram recorded without the sample. The first is then divided by the second to yield the so-called contrast hologram where the influence of illumination inhomogeneities and noise is minimized. To obtain the reconstructed complex object field $E_O(x, y)$, two main groups of numerical reconstruction methods can be applied, according to the distance scales involved, namely, the Rayleigh–Sommerfeld (RS) approximation, for short to intermediate propagation distances, and the Fresnel or paraxial approach, for the long propagation regime. In this case, the propagation distances are of the order of tens of millimetre, which is comparable to the recording sensor size. Therefore, the RS approximation is used in the form of an algorithm consisting of a Fourier Transform (FT) of the digital hologram, the result of which is multiplied by a transfer function, followed by an inverse FT. This is called the Angular Spectrum Method (ASM) [4] and has the advantage of keeping the pixel size independent of the reconstruction distance. After retrieving $E_O(x, y)$, the absolute amplitude $U(x, y) = |E_O(x, y)|$ and the phase $\gamma(x, y) = tan^{-1}\left[\frac{Im\{E_O(x,y)\}}{Re\{E_O(x,y)\}}\right]$ can be computed. For focus evaluation, the absolute amplitude, or alternatively, the intensity $I(x, y) = |E_O(x, y)|^2$ are more often used.

Twenty-two metrics were selected from a preliminary set of focusing metrics that performed well in phase-shifting digital holograms [2] and a study concerning sparsity metrics [11]. Furthermore, these metrics were grouped in four categories according to their mathematical similarities: group A - image statistical/spatial properties-based metrics; group B – wavelet/spectral-based metrics, group C - sparsity metrics, and group D - $l_p - norm$ based sparsity metrics. A detailed description of the focus metrics used in DH and presented herein can be found in recent works [2] [11] [12]. The first group of metrics comprises de following criteria: normalized variance (VAR), the correlation related metrics Vollath's F4 and F5 (VOLF4, VOLF5), the standard deviation correlation function (STDCORR), the differentiation based Tenengrad algorithm (TEN)

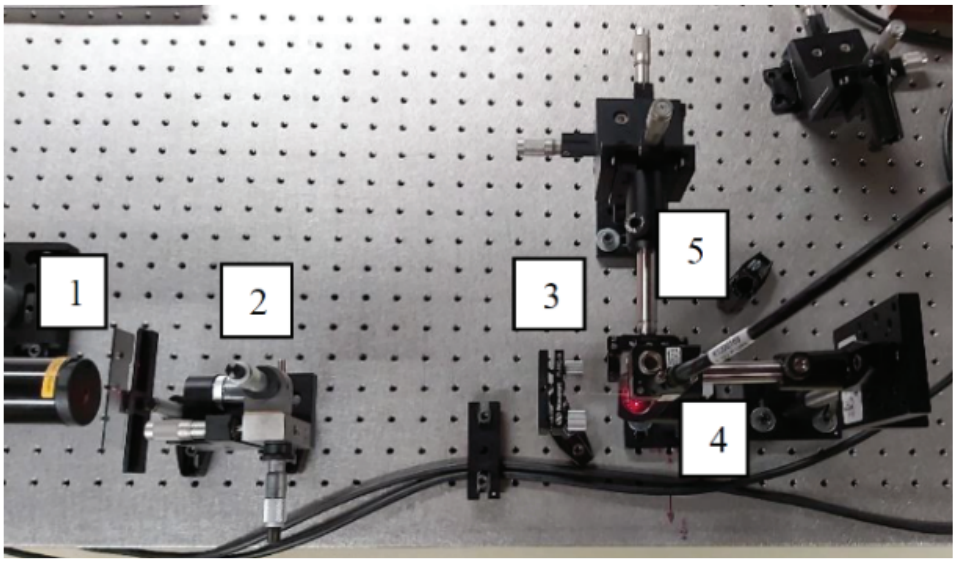

Figure 1: Top view of the inline digital holography setup with vertical camera position. **1**-He-Ne laser ($\lambda = 632.8\ nm$); **2**-Spatial Filter; **3**-Collimating lens; **4**-CMOS camera; **5**-Sample holder.

and Gaussian filter (GF), and finally the energy of the image Laplacian (LAP). The second group includes the wavelets-based focus measures include a decomposition with Daubechies wavelets (WAVRDB6) or with dyadic wavelet using smooth filtering (WAVFILT), the transform-based metrics midfrequency DCT transform metric (MDCT), and the weighted Fourier spectral focus measure (FSL). The third group includes the sparsity related criterion Gini index (GINI), Gaussian entropy (GENTR), Shannon entropy (SHENTR), modified Shannon entropy (MSE), -log (LOG), Kurtosis (KURT) and Hoyer. Finally, in the fourth group are the sparsity-based focus measures l_p (LPNORM), l_1 (L1NORM), l_ϵ^0 (L0EPSNORM), l_2/l_1(L2L1NORM). To compare the results of different focus measures, a set of performance criteria related to unimodality, accuracy (AM), resolution (RM) and range was used. Since only amplitude or mixed amplitude/phase holograms were tested in this study, the above-mentioned metrics, all should yield a maximum at the in-focus position z_f, after proper normalization of the focus curves. The trade-off between performance metrics and computational burthen is also inspected using the mean computation time, at a given step of the search interval, for each of the 22 focus algorithms.

3. Results and discussion

Twenty-two focusing metrics were tested on a calibration object (Fig.2A, USAF 1951 target) and several types of plant fibres from which two were selected: a sample of eucalyptus microfibers (Fig.2B) and a sample of pine tree microfibers (Fig.2C). Since

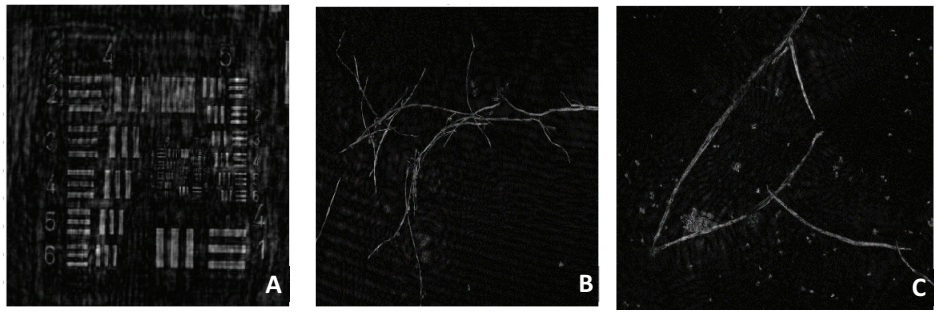

Figure 2: Cropped areas from reconstructed holograms at best focus distances obtained from the average results of the set of focus metrics. (A) USAF1951 (542×545 pixels); (B) Eucalyptus microfibers (1232×947 pixels); and (C) Pine tree microfibers (1403×1070 pixels). Indicated values are the tested resolutions. The displayed resolutions have been squared down to the lowest dimension.

the distances from the camera to the sample holder where small (less than 20 mm), the amplitude spectrum method was used for numerical reconstruction of the acquired holograms. Small distances are recommended for best spatial resolution. The focusing functions were applied to two main sets of data: one using the absolute value of the amplitude of the reconstructed complex fields, $U(x, y) = |E_O(x, y)|$, and another using the corresponding intensity $I(x, y) = |E_O(x, y)|^2$, as this choice has an important influence on the focus performance, as suggested in [11]. The results were compared for each sample, and the amplitude input proved itself a more reliable option, with less cases of failure to identify a peak value. The two sets of data were further divided in two cases regarding reconstruction resolution: one set comprised full-sized reconstructions with square resolutions of 1940×1940 pixels; and a set of interactively selected cropped reconstructions with lower resolutions (in number of pixels) about surrounding de region of interested (ROI) in each case. In the latter case, the idea was to promote a much faster focusing procedure without sacrificing the focusing performance. The second approach, not only revealed to be faster, but also more effective in most cases. Thus, the following presented results relate mainly to the case of cropped ROIs of amplitude inputs to the tested focus functions.

Table 1 was selected from a set of results to illustrate the behaviour of the tested metrics when using an object with different scales of resolution such as the USAF 1951 target, ranging from 1 to 645 pair of lines per mm. The focusing criteria outcomes for the Eucalyptus microfibers sample are also shown for comparison. Using the USAF 1951 target also allowed an appraisal of the resolution capability of the setup used in this work. Figures 3 to 5 show the behaviour of the focus metrics, grouped as previously described, for the resolution target and the two types of microfibers presented in Fig. 2. The focusing curves obtained from Eucalyptus microfibres samples showed a smoother behaviour except for the GINI index and the l_ϵ^0 norm. This is likely due to less abrupt

Table 1: Performance of focusing criteria for the cropped areas of a USAF 1951 target and Eucalyptus microfibers shown in Fig.2A and Fig.2B, respectively. The three most performing metrics values in terms of accuracy (AM- accuracy metric), fidelity to the true value and resolution (RM-resolution metric), while identifying the correct z_f, are highlighted. All values in millimetres.

Metrics	USAF 1951			Eucalyptus microfibers			Pine tree microfibers		
	AM	z_f	RM	AM	z_f	RM	AM	z_f	RM
VAR	0.050	17.67	0.121	0.044	18.36	0.099	0.104	17.73	0.148
VOLF4	0.026	17.71	0.076	0.032	18.37	0.088	0.034	17.71	0.123
VOLF5	0.037	17.66	0.127	0.053	18.36	0.102	0.100	17.75	0.147
STDCORR	0.054	17.67	0.124	0.046	18.36	0.102	0.103	17.78	0.148
TEN	0.025	17.67	0.090	0.028	18.36	0.082	0.036	17.71	0.129
GF	0.126	17.72	0.123	0.082	18.38	0.114	0.091	17.78	0.145
LAP	0.004	17.65	0.114	0.015	18.35	0.059	0.106	17.79	0.170
WAVRDB6	0.050	17.68	0.108	0.035	18.36	0.087	0.040	17.72	0.121
WAVRFILT	0.015	17.66	0.127	0.010	18.35	0.068	0.009	17.80	0.135
MDCT	0.016	17.67	0.046	0.022	18.36	0.064	0.025	17.71	0.135
FSL	0.004	17.65	0.121	0.017	18.36	0.056	0.050	17.68	0.161
GINI	0.039	17.66	0.121	0.025	18.41	0.157	0.098	17.79	0.155
GENTR	0.048	17.67	0.119	0.051	18.36	0.101	0.096	17.79	0.150
SHENTR	0.049	17.67	0.119	0.044	18.36	0.098	0.102	17.73	0.145
MSHENTR	0.044	17.67	0.118	0.043	18.36	0.100	0.103	17.79	0.149
LOG	0.054	17.70	0.121	0.048	18.36	0.103	0.000	17.77	0.147
KURT	0.050	17.70	0.122	0.051	18.36	0.101	0.103	17.73	0.147
HOYER	0.049	17.67	0.119	0.044	18.36	0.098	0.102	17.73	0.145
L0EPSNORM	0.007	17.67	0.120	0.002	18.11	0.290	0.000	18.10	0.406
LPNORM	0.050	17.70	0.121	0.046	18.36	0.101	0.103	17.79	0.149
L1NORM	0.053	17.70	0.124	0.045	18.36	0.102	0.102	17.78	0.148
L2L1NORM	0.051	17.67	0.121	0.044	18.36	0.099	0.105	17.73	0.149

refractive index changes and consequent absence of speckle noise, as shown in Fig. 2. The LAP and the FSL metrics yield the best accuracy value (AM) for all the tested samples. However, they fail to fulfil the unimodality criterion over most of the samples. Wider metrics such as the VAR, or sparsity based l_p and l_1 norms, tend to be more reliable, although they may not be so useful when the separation of different layers with individual particles or features is intended, such as in particle tracking applications.

Another important aspect of a focus metric's performance is its computational complexity. Thus, to assess the efficiency of each algorithm, the mean and standard deviation of the computation time for the calculation each focus measure for a given step of the search interval was computed. The tests were performed on the USAF 1951 reconstructions with 1940×1940 pixels. All codes were developed with MATLAB R2018b, using a Pentium core i7 – 4720HQ at 2.6 GHz (four cores. eight logical processors). It can be

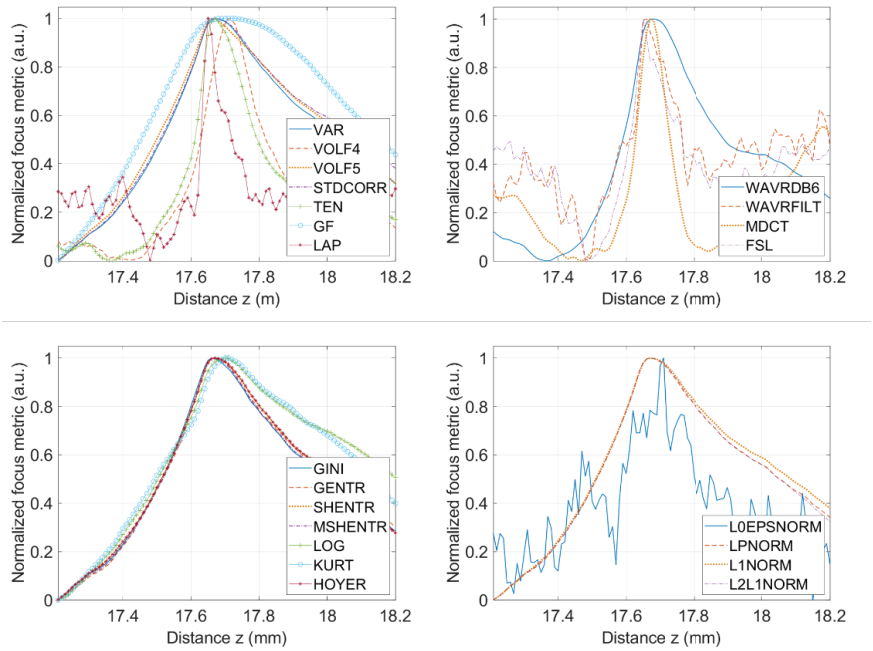

Figure 3: Comparative assessment of focusing metrics from group A to group D using the cropped area of the USAF 1951 target. All the represented metrics were able to identify a sharp peak near the true value determined by visual inspection. The search interval contained 100 points with a step size 20 µm over a range of $[17.2.\ 18.2]$ mm.

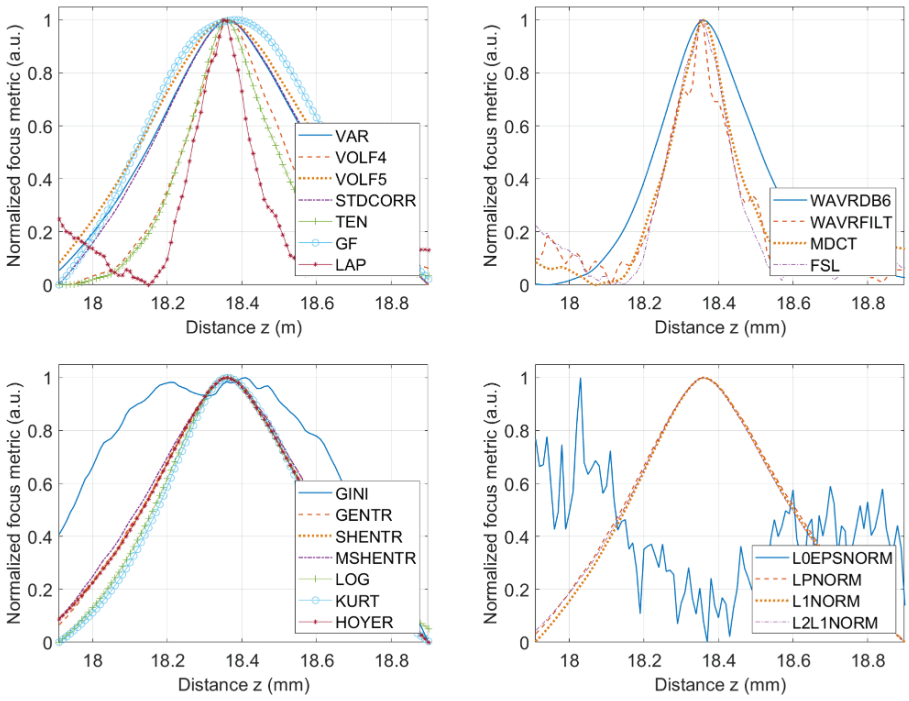

Figure 4: Comparative assessment of focusing metrics from group A to group D using the cropped area of Eucalyptus microfibers. The search interval contained 100 points. with a step size of 10 μm. over a range of [17.8.18.8] mm. All the represented metrics were able to identify a sharp peak near the true value, except for the l_ϵ^0 norm.

observed that among the most performing metrics in terms of correct identification of the

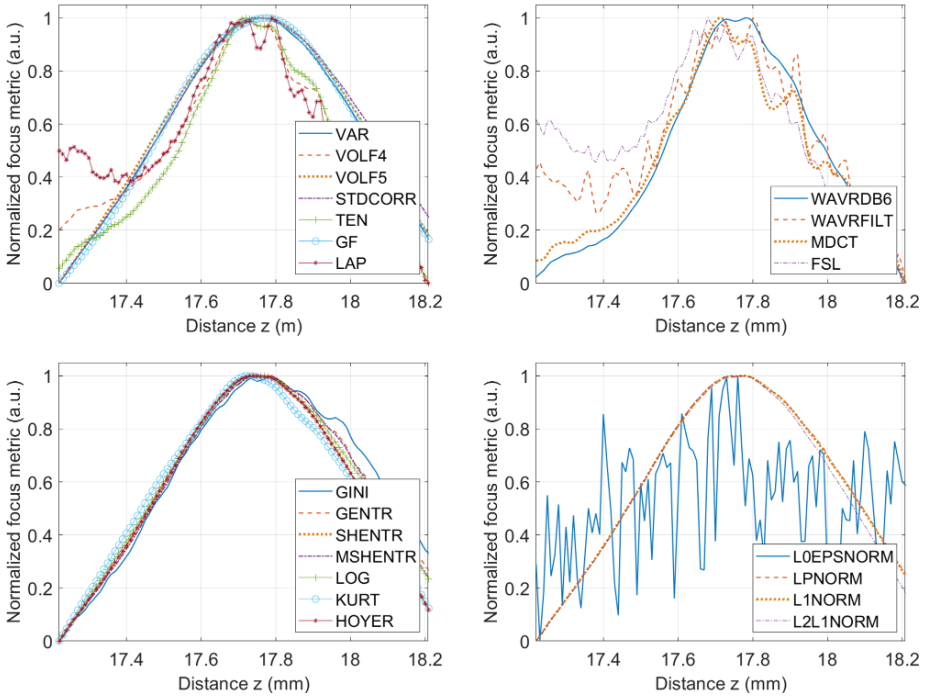

Figure 5: Focus curves comparison for the sample of Pine tree microfibers. The search interval contained 100 points. with a step size of 10 μm. over a range of [17.2.18.2] mm. As in the previous sample, all but the l_{ϵ}^{0} norm have successfully identified the focus distance.

focus distance, the sparsity-based metrics l_p and l_1, and l_2/l_1 norms have the additional advantage of being very fast. Furthermore, as pointed out earlier, these metrics are widely employed in compressive sensing methods, thus showing a promising value in the development of a new simultaneous reconstruction/focusing method for improved resolution and noise reduction.

4. Conclusions

The present results illustrate the importance of choosing a highly performing autofocus method for in-line digital holography of plant microfibers. The nature of each tested sample has an impact in this choice. with diversity of feature size and axial location of different objects within the sample leading to stronger differences between focus criteria. For a coarse initial location of a given microstructure, faster and more robust, but less precise metrics such as the VAR, or sparsity based l_p and l_1 norms, tend to be more reliable and can be embedded in compressive sensing algorithms. The Laplacian (LAP) and the Fourier spectral focus measure (FSL) metrics yield the best accuracy value, but can only be applied to narrow range intervals, due to the lack of unimodality. More elaborated metrics, such as the dyadic wavelet using smooth filtering (WAVRFILT), help

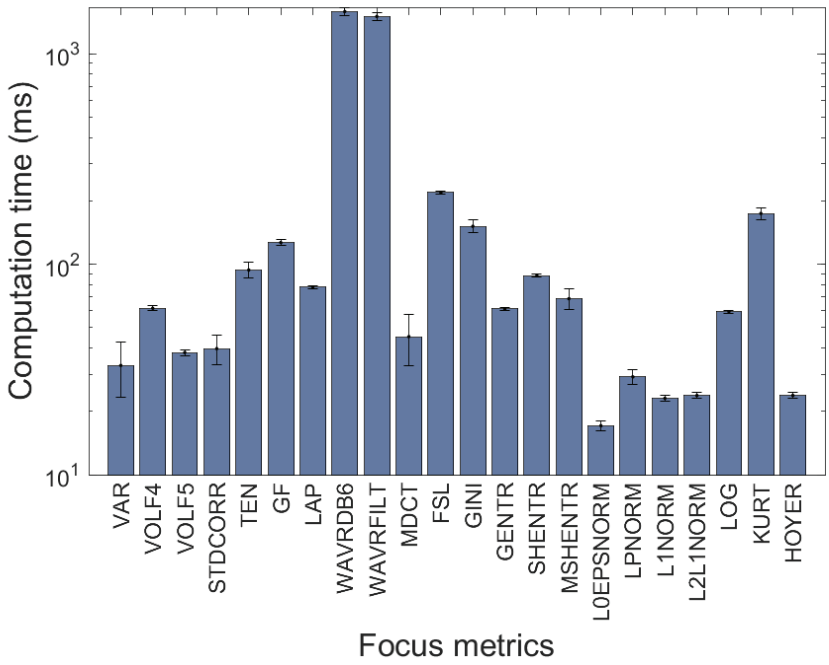

Figure 6: Mean and standard deviation of the computation time, at a given step of the search interval, for each of the 22 focus measures when applied to the reconstruction of the USAF 1951 target.

distinguishing structures buried at distinct depths, at the cost of a high computation complexity. Regarding future work, a comparative study of autofocus methods using an in-line digital holographic microscopy setup is in progress. Preliminary results show that magnified holograms are more demanding in terms of autofocus robustness to misalignment and noise issues. In this case, the statistically based metrics such as the variance (VAR) and Vollath's F5 (VOLF5), and the sparsity-based metrics such as the Gini Index (GINI) have shown better performance, so far.

References

[1] Hong XYJ, Liu C, Kim MK. Review of digital holographic microscopy for three-dimensional profiling and tracking. Optical Engineering, 2014, 53.11:112306-1.

[2] Fonseca ES, Fiadeiro PT, Pereira M, Pinheiro A. Comparative analysis of autofocus functions in digital in-line phase-shifting holography. Applied Optics, 2016, 55.27: 7663-7674.

[3] Kim MK. Applications of digital holography in biomedical microscopy. Journal of the Optical Society of Korea, 2010, 14.2: 77-89.

[4] Ting-Chung O, Jung-Poon L. Introduction to modern digital holography. UK: Cambridge University Press; 2014.

[5] Marulier C, Dumont P, Orgéas L, Roscoat SR. Towards 3D analysis of pulp fibre networks at the fibre and bond levels. Nordic Pulp and Paper Research Journal, 2012, 27.2: 245-255.

[6] Chhaniwal V, Singh AS. Leitgeb RA, Javidi B, Anand A. Quantitative phase-contrast imaging with compact digital holographic microscope employing Lloyd's mirror. Optics letters, 2012, 37.24: 5127-5129.

[7] Malek M, Khelfa H, Picart P, Mounier D, Poilâne C. Microtomography imaging of an isolated plant fiber: A digital holographic approach. Applied Optics, 2016, 55.3:111-121.

[8] Ma X, Xiao W, Pan F. Reconstruction method for samples with refractive index discontinuities in optical diffraction tomography. Optics and Lasers in Engineering, 2017, 94: 58-62.

[9] Wahba H, Sjödahl M, Gren P, Olsson E. High resolution digital holographic microscopy for the study of aggregated natural cellulose nanowhisker fibers. Optics and Lasers in Engineering, 2015, 73: 69-74.

[10] Zhang Y, Huang Z, Jin S, Cao L. Autofocusing of in-line holography based on compressive sensing. Optics and Lasers in Engineering. 2021, 146. 106678-1.

[11] Xin F, Healy J, Hennelly B. Investigation of sparsity metrics for autofocusing in digital holographic microscopy. Optical Engineering, 2017, 56.5: 053112-1.

[12] Mohamed S, Bouamama L, Bahloul D, Picart P. Quality assessment of refocus criteria for particle imaging in digital off-axis holography. Applied Optics, 2017, 56.13: 158-166.